Spinodal decomposition: A survey of recent results

Stanislaus Maier-Paape
Institut für Mathematik
Universität Augsburg
86135 Augsburg, Germany

Evelyn Sander
Department of Mathematical Sciences
George Mason University
Fairfax, VA 22030, USA

Thomas Wanner
Department of Mathematics and Statistics
University of Maryland, Baltimore County
Baltimore, MD 21250, USA

Abstract

This paper describes recent mathematical progress explaining the phenomenon of spinodal decomposition in metal alloys as modeled by the Cahn-Hilliard equation. We discuss work on the early stages of this decomposition due to Maier-Paape, Wanner [25, 26], results on later stages due to Sander, Wanner [28, 29], as well as applications to multi-component alloys due to Maier-Paape, Stoth, Wanner [24].

1 Introduction

Spinodal decomposition is an intriguing phenomenon in the study of metal alloys [8, 20, 22]: If a homogeneous high-temperature mixture of two metallic components is rapidly quenched to a certain lower temperature, then a sudden phase separation sets in. The mixture quickly becomes inhomogeneous and forms a characteristic but non-periodic structure.

In order to describe this phase separation process (as well as other phenomena) Cahn and Hilliard [6, 9] proposed the fourth-order parabolic partial differential equation

$$\begin{aligned} u_t &= -\Delta(\epsilon^2 \Delta u + f(u)) \quad \text{in} \quad \Omega\,, \\ &\frac{\partial u}{\partial \nu} = \frac{\partial \Delta u}{\partial \nu} = 0 \quad \text{on} \quad \partial\Omega \end{aligned} \tag{1}$$

for the concentration u of one of the metals as a function of space and time, where u is affine scaled to be between -1 and 1. (Since the total concentration is always 1, the concentration of the other metal is then uniquely determined as well.)

The domain $\Omega \subset \mathbb{R}^n$ is bounded with appropriately smooth boundary, $n \in \{1, 2, 3\}$, and the function $-f$ is the derivative of a double-well potential F, the standard example

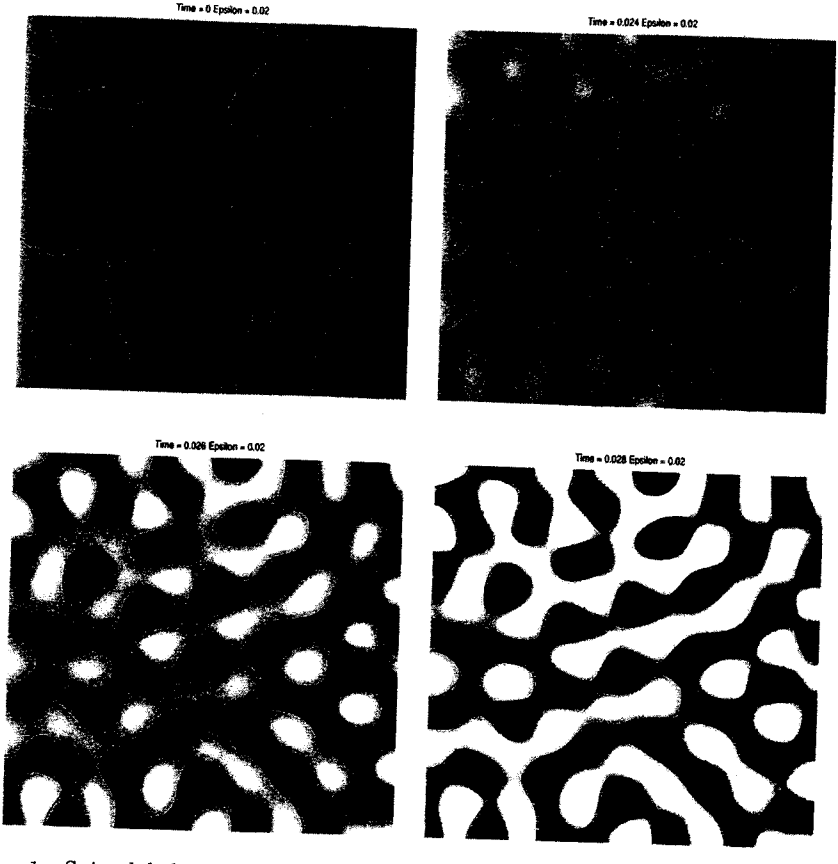

Figure 1: Spinodal decomposition in two dimensions for $\varepsilon = 0.02$. Color represents concentration, with black corresponding to all one metal, white to all the other metal, and gray a mixture of the two metals.

being the cubic function $f(u) = u - u^3$. ε is a small positive parameter modeling interaction length. The Cahn-Hilliard equation is *mass-conserving*, i.e., the total concentration $\int_\Omega u dx$ remains constant along any solution u. Moreover, it is an $H_0^{-1}(\Omega)$-*gradient system* with respect to the van der Waals free energy functional

$$E_\varepsilon[u] := \int_\Omega \left(\frac{\varepsilon^2}{2} \cdot |\nabla u|^2 + F(u) \right) dx \,,$$

where F is the double-well potential mentioned above, see Fife [18].

Every constant function $\bar{u}_o \equiv \mu$ is a stationary solution of (1). Spinodal decomposition corresponds to this equilibrium being unstable. This occurs in the (usually connected)

set of all $\mu \in \mathbb{R}$ such that $f'(\mu) > 0$, known as the spinodal interval. Thus any orbit originating near $\bar{u}_o$ is likely to be driven away from this equilibrium. Explaining precisely how this happens lies at the heart of explaining the phenomenon of spinodal decomposition. A two-dimensional simulation of this process is pictured in Figure 1.

There have been many papers in the physics literature dealing with spinodal decomposition and how it is modeled by the Cahn-Hilliard equation. We refer the reader to Cahn [7, 8], Hilliard [20], Langer [22], Elder, Desai [12], Elder, Rogers, Desai [13], and Hyde et al. [21], just to name a few. Also, there exist numerous papers on numerical simulations of the Cahn-Hilliard equation, see for example Elliott, French [15], Elliott [14], Copetti, Elliott [11], Copetti [10], and Bai et al. [1, 2].

This survey paper describes the mathematical treatment of spinodal decomposition contained in several of our recent papers. We have used a dynamical approach, taking the point of view that in order to understand spinodal decomposition, one must consider the behavior of the nonlinear solutions by comparison to linear behavior on a dominating subspace. Section 2 of this survey describes the linearization of the Cahn-Hilliard equation, and how Maier-Paape and Wanner [25] used this to understand the size of spinodal patterns. Since ε models a small materials dependent effect on the atomic level, one considers asymptotic results as ε tends to zero. Building on the linear results, Section 3 describes the early decomposition process of (1) due to Maier-Paape, Wanner [25, 26]. The goal is to find a starting radius r_ε and an ending radius R_ε of a physically relevant size so that one can explain the occurrence of spinodal decomposition for most solutions starting within distance r_ε from the equilibrium, until they reach distance R_ε. These results are an improvement on the one-dimensional results of Grant [19]; Section 3 compares the two results. Sander and Wanner [28, 29] further extended the explanation of the behavior of solutions described in [26] to give a picture of the later stages of spinodal decomposition; see Section 4. The final section of this survey reviews how these ideas can be applied to Cahn-Hilliard systems, corresponding to alloys of more than two metals. Maier-Paape, Stoth, and Wanner [24] adapted the early stage decomposition to the system case. Eyre, Maier-Paape, Sander, and Wanner intend to extend the later stages results to the systems case as well. We also indicate how these results apply to related equations. Note that throughout the paper, we have removed as many technical details as possible; please refer to the papers listed in the references to see the full statements of the results.

2 Linear results and wavelength estimate

Linearizing (1) at $\bar{u}_o \equiv \mu$ gives the linear equation

$$\begin{aligned} v_t \;=\; A_\varepsilon v \;:=\; -\Delta(\varepsilon^2 \Delta v + f'(\mu) v) \quad &\text{in} \quad \Omega\,, \\ \frac{\partial v}{\partial \nu} = \frac{\partial \Delta v}{\partial \nu} = 0 \quad &\text{on} \quad \partial\Omega\,, \end{aligned} \tag{2}$$

where A_ε is considered as an operator on the subspace X of $L^2(\Omega)$ consisting of functions with total mass zero. Let $0 < \kappa_1 \le \kappa_2 \le \ldots \to +\infty$ and $\psi_1, \psi_2, \ldots$ denote the eigenvalues and eigenfunctions of the operator $-\Delta$ on the same domain subject to Neumann boundary

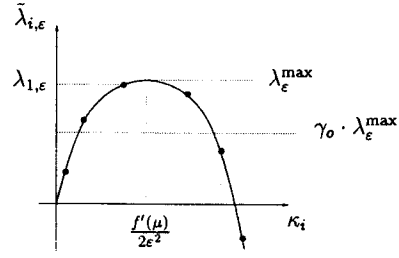

Figure 2: Eigenvalues of the linearization A_ε.

conditions. Then the ψ_i are eigenfunctions of (2), with corresponding eigenvalues

$$\tilde{\lambda}_{i,\varepsilon} := \kappa_i(f'(\mu) - \varepsilon^2\kappa_i) \,, \quad i \in \mathbb{N} \,.$$

By reordering the numbers $\tilde{\lambda}_{i,\varepsilon}$ we obtain the spectrum of A_ε, which consists of the eigenvalues $\lambda_{1,\varepsilon} \geq \lambda_{2,\varepsilon} \geq \ldots \to -\infty$. This spectrum is bounded above by

$$\lambda_\varepsilon^{\max} := \frac{f'(\mu)^2}{4\varepsilon^2} \,,$$

and the largest eigenvalue $\lambda_{1,\varepsilon}$ of A_ε is proportional to $\lambda_\varepsilon^{\max}$, see Figure 2. Moreover, the eigenfunctions form a complete $L^2(\Omega)$-orthogonal set in X. The strongest unstable directions correspond to $\kappa_i \approx f'(\mu)/(2\varepsilon^2)$. Most solutions of (2) originating near zero will be driven away in these unstable directions, as Cahn pointed out in [7]. As a result, we define the *dominating subspace* $\mathcal{Y}_\varepsilon^+$ as

$$\mathcal{Y}_\varepsilon^+ = \text{span}\left\{\psi_k : \tilde{\lambda}_{k,\varepsilon} > \gamma_0 \cdot \lambda_\varepsilon^{\max}\right\} \tag{3}$$

for some $\gamma_0 < 1$ close to one. Note however that the unstable spectrum of the linearization is not the full story for the nonlinear equation, as one would expect extremely large nonlinear effects due to a Laplacian applied to a cubic term.

Most solutions of the linearized equation will remain close to $\mathcal{Y}_\varepsilon^+$, i.e., their geometry resembles the geometry of functions in $\mathcal{Y}_\varepsilon^+$ (cf. [25, Section 2]). Maier-Paape and Wanner also proved that these functions exhibit a common wavelength which is of the order of ε, see [25, Section 4]. Specifically, at fixed time t, the level set $\{u(x,t) = 0\}$ divides Ω into a set where u is positive, and a set where u is negative. These two sets are called nodal domains. The following theorem describes the width of the nodal domains, explaining why these domains are typically thin:

Theorem 2.1 *Let $\varphi \in \mathcal{Y}_\varepsilon^+$ be arbitrary, and let $x_0 \in \Omega$ denote a "typical" point. If $G \subset \Omega$ denotes the nodal domain of φ containing x_0, then for any ball contained in G with radius r and center x_0 we have $r \leq C \cdot \varepsilon$.*

3 Early stages of the decomposition

Nonlinear analysis of the Cahn-Hilliard equation uses the information gained from the linearization, combined with the fact that the Cahn-Hilliard equation generates a nonlinear semiflow on the $H^2(\Omega)$-functions of fixed mass satisfying the boundary conditions. $H^2(\Omega)$ is the Hilbert space of functions with two weak derivatives in $L^2(\Omega)$. Since this is the mathematically relevant space, unless otherwise specified all distances are with respect to the $H^2(\Omega)$-norm. Grant [19] described spinodal decomposition for one-dimensional domains Ω, showing that for generic small ε, most solutions of (1) starting in a sufficiently small neighborhood U_ε of size r_ε of $\bar{u}_o \equiv \mu$ closely follow a strongly unstable one-dimensional manifold for a long time. This unstable manifold is tangent to the eigenfunction $\varphi_{1,\varepsilon}$ of the largest eigenvalue $\lambda_{1,\varepsilon}$, which is simple for generic values of ε. Grant also proved that the two branches of the strongly unstable manifold converge to periodic equilibrium points of (1), whose period is proportional to ε as $\varepsilon \to 0$ and whose $L^\infty(\Omega)$-norm is bounded away from zero. Thus most nearby orbits undergo phase separation with the characteristic wavelength ε.

Unfortunately, for higher-dimensional domains Grant's approach predicts evolution of most orbits towards regular patterns which are not observed in practice. Maier-Paape and Wanner [25, 26] pointed out that this discrepancy is due to the fact that r_ε in Grant's result is of the order $\exp(-c/\varepsilon^2)$. Since ε models interaction length, an effect which occurs on the atomic level, it is extremely small. Thus, the behavior of solutions described by Grant cannot be observed in the physical system. To address this, Maier-Paape and Wanner proposed a different approach for explaining spinodal decomposition, which applies to two- and three-dimensional domains Ω as well. They also consider solutions of (1) starting in a ball U_ε of radius r_ε of the homogeneous equilibrium $\bar{u}_o \equiv \mu$. This time however, the size r_ε of U_ε is proportional to $\varepsilon^{\dim\Omega}$.

More precisely, inside a ball W_ε of radius R_ε, where R_ε is proportional to $\varepsilon^{\dim\Omega}$, there is a finite-dimensional inertial manifold $\mathcal{N}_\varepsilon$, with dimension proportional to $\varepsilon^{-\dim\Omega}$, which exponentially attracts all orbits in W_ε. As a result, to understand the behavior of solutions within W_ε, one only needs to consider the behavior of solutions within $\mathcal{N}_\varepsilon$. Maier-Paape and Wanner [26] show that starting inside an even smaller ball U_ε of radius $r_\varepsilon < R_\varepsilon$ around $\bar{u}_o$, where r_ε is also proportional to $\varepsilon^{\dim\Omega}$, one can reduce the dimension of the problem even further; the behavior of solutions in U_ε is dominated by a manifold $\mathcal{M}_\varepsilon \subset \mathcal{N}_\varepsilon$, in the sense that most solutions starting in U_ε leave W_ε close to $\mathcal{M}_\varepsilon$. The dimension of $\mathcal{M}_\varepsilon$ is proportional to $\varepsilon^{-\dim\Omega}$, yet considerably smaller than the dimension of $\mathcal{N}_\varepsilon$. Furthermore $\mathcal{M}_\varepsilon$ is close to the dominating linear subspace $\mathcal{Y}_\varepsilon^+$ introduced in Section 2. See Figure 3.

To prove these results, one first looks at abstract semilinear parabolic equations of the form

$$u_t = Au + F(u) \tag{4}$$

with stationary state $\bar{u}_o$ generating semiflows in fractional power spaces. Assuming the existence of certain spectral gaps for the linear part A, whose size is suitably related to a small global Lipschitz constant of the nonlinear part F, results on invariant manifolds and foliations are used to establish the existence of a "power law," which states that solutions of (4) leaving a given neighborhood of $\bar{u}_o$ far away from a strongly unstable manifold must

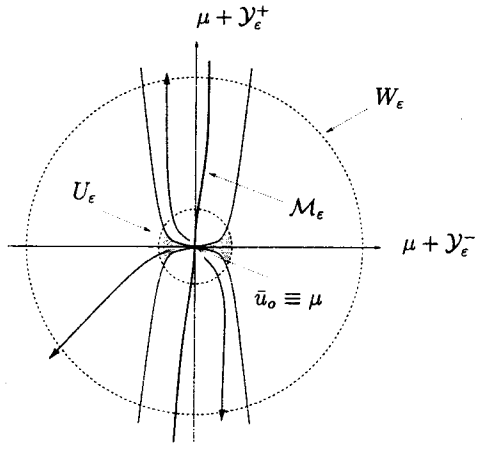

Figure 3: The early stages of decomposition.

lie outside a parabolically-shaped graph (the shaded region in Figure 3). In combination with some technical estimates, this implies the dominating effects of a strongly unstable manifold on solutions originating sufficiently close to $\bar{u}_o$.

The fact that most solutions of (1) originating in U_ε exit W_ε close to $\mathcal{Y}_\varepsilon^+$ fully explains spinodal decomposition inside W_ε. Moreover, in the previous section we showed that solutions within $\mathcal{Y}_\varepsilon^+$, as well as nearby, exhibit the same spinodal decomposition patterns which are observed in experiments.

Although the above approach predicts the correct patterns observed in spinodal decomposition, the result is still not optimal. R_ε is proportional to $\varepsilon^{\dim\Omega} \ll 1$. In practice however, the predicted patterns are observed until the maximum norm of the solution is of order one.

4 Later stages of the decomposition

Motivated by the existence of a dominating linear subspace, Sander and Wanner [28] did numerical simulations to compare a solution v of the linear Cahn-Hilliard equation (2) such that $v(x,0) = u_o(x)$, and solution u of the nonlinear Cahn-Hilliard equation (1) satisfying the same initial condition: $u(x,0) = u_o(x)$. Simulations in one space dimension indicate that the relative distance $||u-v||_{H^2(\Omega)}/||v||_{H^2(\Omega)}$ between the nonlinear solution u and the linear solution v remains bounded by some small ε-independent threshold, as long as the $H^2(\Omega)$-norm of the nonlinear solution is approximately bounded by $C\varepsilon^{-2}$. Figure 4 shows the maximal norm of u such that the relative distance remains below 0.5% as a function of ε, given in both the $H^2(\Omega)$- and $L^\infty(\Omega)$-norms (100 simulations for each ε).

The insight given by this numerics led to the following theorem from Sander and Wanner [29]:

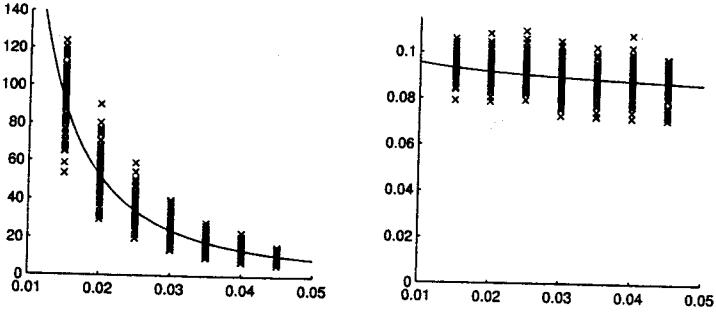

Figure 4: Dependence of the maximal radius R (vertical axis) on ε (horizontal axis) with respect to a norm equivalent to the $H^2(\Omega)$-norm (left) and the $L^\infty(\Omega)$-norm (right) for the domain $\Omega = (0,1)$, and relative error 0.5%. Figure from [28].

Theorem 4.1 *Consider the Cahn-Hilliard equation (1) in dimension 1, 2, or 3 with* $f(u) = u - u^3$ *and* $\mu = 0$. *Let* $\varrho > 0$ *be arbitrarily small, but fixed. Let* u_o *denote an initial condition polynomial in* ε *close to* $\bar{u}_o \equiv \mu$, *and which is sufficiently close to the dominating subspace* $\mathcal{Y}_\varepsilon^+$. *Finally, let* u *and* v *be the solutions to (1) and (2), respectively, starting at* u_o. *Then as long as*

$$||u(t)||_{H^2(\Omega)} \leq C \cdot \varepsilon^{-1+\varrho+\dim\Omega/4} \cdot ||u_o||^\varrho_{H^2(\Omega)} \tag{5}$$

we have

$$\frac{||u(t) - v(t)||_{H^2(\Omega)}}{||v(t)||_{H^2(\Omega)}} \leq C \cdot \varepsilon^{2-\dim\Omega/2} .$$

In other words, u *remains extremely close to* v *until* $||u(t)||_{H^2(\Omega)}$ *exceeds the threshold given in (5).*

Note that the radius of the starting domain can be chosen to be polynomial in ε, and thus physically visible, and that the threshold given in (5) grows as $\varepsilon \to 0$.

The proof of this theorem comes from restricting attention to functions near the dominating linear subspace. That is, choose a dominating subspace $\mathcal{Y}_\varepsilon^+$ as in (3). Let $\mathcal{Y}_\varepsilon^-$ be the orthogonal complement of the dominating space, spanned by the eigenfunctions not contained in $\mathcal{Y}_\varepsilon^+$. Functions "near" $\mathcal{Y}_\varepsilon^+$ are those lying in an unstable cone of $\mathcal{Y}_\varepsilon^+$ of small opening δ. That is,

$$\mathcal{C}_\delta = \left\{ u = u^+ + u^- \in \mathcal{Y}_\varepsilon^+ \oplus \mathcal{Y}_\varepsilon^- \ : \ ||u^-||_{H^2(\Omega)} \leq \delta \cdot ||u^+||_{H^2(\Omega)} \right\} .$$

On this unstable cone, it is possible to find a precise upper bound in terms of ε on the nonlinearity. Combining this with an application of Gronwall's Lemma, one can restrict the growth rate of the relative distance between u and v. Furthermore, since the linear solution v always remains in the cone, it is possible to find a lower bound on the norm of u up to which the solution does not exit the cone. This gives the estimate for the exit radius R as a function of ε. Note that we do not need to use any spectral gap condition.

This theorem furnishes an explanation for a mechanism underlying spinodal decomposition. Namely, if a solution of the nonlinear Cahn-Hilliard equation starts near the dominating subspace sufficiently close to the homogeneous equilibrium $\bar{u}_o \equiv \mu$, it will follow the corresponding solution of the linearized equation for a long time. Thus, the patterns observed during spinodal decomposition are precisely the patterns generated by the linearized evolution. This is unexpected; as mentioned before, the nature of the equation throughout most of the space is highly nonlinear.

Theorem 4.1 considers only initial conditions u_o lying in a small cone $\mathcal{C}_\delta$ centered around $\mathcal{Y}_\varepsilon^+$. Fortunately, due to Section 3 this is exactly the region where most solutions originating near $\bar{u}_o \equiv \mu$ end up automatically. Thus, combining the results of Maier-Paape and Wanner [25, 26] with Theorem 4.1 immediately gives the following theorem:

Theorem 4.2 *Consider (1) for $f(u) = u - u^3$ and $\mu = 0$, and let $\varrho > 0$ be arbitrary, but fixed. If we randomly choose an initial condition u_o satisfying*

$$\|u_o\|_{H^2(\Omega)} \leq C \cdot \varepsilon^k \,,$$

where $k > 0$ depends on ϱ and $\dim \Omega$, then with high probability, the solution u of (1) originating at u_o will closely follow the solution of the linearized equation as long as

$$\|u(t)\|_{H^2(\Omega)} \leq C \cdot \varepsilon^{-1+\varrho+\dim\Omega/4} \,. \tag{6}$$

In other words, with high probability, solutions behave almost linearly for a long time for small ε.

The results of this section can easily be generalized to other nonlinearities f. In fact, better values for the radii given in (5) and (6) can be obtained in this way. Consider for example the case $f_\sigma(u) = u - u^{1+\sigma}$, where $\sigma \geq 1$. The corresponding double-well potentials F_σ are given by $F_\sigma(u) = u^{2+\sigma}/(2+\sigma) - u^2/2$. Notice that for $\sigma \to \infty$ these potentials approach the non-smooth free energy which has been discussed by Blowey and Elliott [4, 5]. For $\mu = 0$ and a nonlinearity of this form, the radius in (6) can be replaced by

$$C \cdot \varepsilon^{(-2+\dim\Omega/2)\cdot(1-1/\sigma)+\varrho} \,.$$

A similar statement is valid for the radius given in (5). Thus, by choosing a suitable double-well potential F_σ, we can get as close to the order $\varepsilon^{-2+\dim\Omega/2}$ as we wish.

These results for binary alloys still leave a number of open avenues of study. For example, Theorem 4.2 does not give the exponent -2 seen in the one-dimensional simulations, but it is conjectured that rather than using a cone, if we were to make a more careful choice of functions "near" $\mathcal{Y}_\varepsilon^+$, the threshold to which nearly linear behavior dominates would be closer to the numerically computed exponent. Further, the numerical results displayed in Figure 4 indicate that there should be a statement similar to Theorem 4.1 linking the region of almost linear behavior to the $L^\infty(\Omega)$-norm.

5 Future directions

So far, all results discussed are for alloys with two metals. Experimental evidence shows that spinodal decomposition can also be observed for multi-component alloys. That is, a

homogeneous mixture of $N \geq 3$ components, when rapidly quenched, can separate into phases with a characteristic wavelength. In this situation, the phases are not regions of concentration of one metal; each is a mixture of the components. To model this, Morral and Cahn [27] introduced the system

$$\begin{aligned} \frac{\partial u_i}{\partial t} &= -\Delta(\varepsilon^2 \Delta u_i + f_i(u_1, \ldots, u_N)) \quad \text{in} \quad \Omega\,, \\ \frac{\partial u_i}{\partial \nu} &= \frac{\partial \Delta u_i}{\partial \nu} = 0 \quad \text{on} \quad \partial\Omega\,, \end{aligned} \tag{7}$$

for $i = 1, \ldots, N$. Since the total concentration is one, we always have the additional constraint that

$$\sum_{i=1}^{N} u_i(x,t) = 1\,,$$

i.e., the values of the vector $u = (u_1, \ldots, u_N)$ describing the composition of the alloy are contained in the so-called *Gibbs simplex* $\mathcal{G}$ defined by

$$\mathcal{G} := \left\{ v \in \mathbb{R}^N \,:\, \sum_{i=1}^{N} v_i = 1\,,\ v_i \geq 0\,,\ i = 1, \ldots, N \right\}\,.$$

Generalizing the previous situation, the standard nonlinearity $f = (f_1, \ldots, f_N)$ is essentially the negative derivative of an N-well potential F, the standard example being

$$F(u_1, \ldots, u_N) = \sigma \cdot \sum_{i<j} u_i u_j + \sum_{i=1}^{N} u_i \ln u_i\,. \tag{8}$$

See Eyre [16, 17] for numerical simulations and a linear analysis of spinodal decomposition for (7) with the above nonlinearity.

The spectrum of the linearized system at a spatially homogeneous equilibrium $\bar{u}_o \in \mathcal{G}$ is a close analogue to the scalar case (1). Namely, eigenfunctions are of the form $\vec{w}_k \cdot \psi_i$ for $k = 1, \ldots, N-1$ and $i \in \mathbb{N}$, where the ψ_i are (scalar-valued) eigenfunctions of $-\Delta$, and the $\vec{w}_k$ are eigenvectors for a constant matrix B within the linearization of (7) with corresponding eigenvalues $\beta_1 \geq \ldots \geq \beta_{N-1}$. The resulting eigenvalues of the linearization of (7) are of the form

$$\tilde{\lambda}_{i,k,\varepsilon} = \kappa_i \cdot \left(\beta_k - \varepsilon^2 \kappa_i\right)\,.$$

Thus, each eigenvector $\vec{w}_k$ corresponds to a curve of eigenvalues as in Figure 2, all curves being bounded by some $\lambda_\varepsilon^{\max}$. Furthermore, the homogeneous equilibrium $\bar{u}_o \in \mathcal{G}$ is unstable if $\beta_1 > 0$. For the nonlinearity given in (8) and $N = 3$ this occurs if $\bar{u}_o$ is contained in the shaded regions shown in Figure 5. The corners e_i of the triangle correspond to the three pure states of the material.

Maier-Paape, Stoth, Wanner [24] showed that using an analogous dominating subspace $\mathbb{Y}_\varepsilon^+$ as in the scalar case, i.e.,

$$\mathbb{Y}_\varepsilon^+ := \operatorname{span}\left\{ \vec{w}_k \cdot \psi_i : \tilde{\lambda}_{i,k,\varepsilon} > \gamma_0 \cdot \lambda_\varepsilon^{\max} \right\}$$

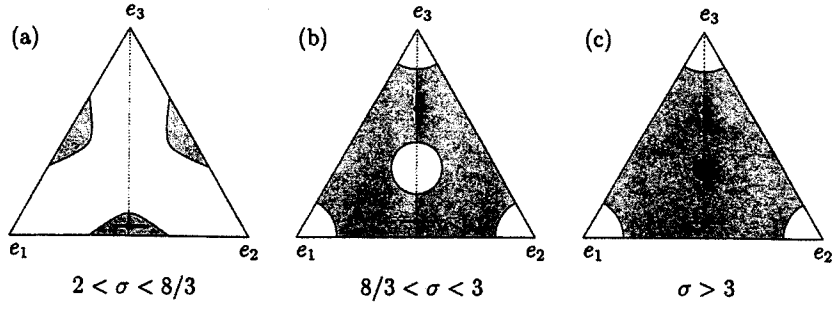

Figure 5: Directions of the dominating subspaces $\mathbb{Y}_\varepsilon^+$.

for some $\gamma_0 < 1$ close to one, the results on the early stages of spinodal decomposition also apply to the system case. Notice that if $\mathcal{Y}_\varepsilon^+$ denotes an appropriate dominating subspace of the binary case as introduced in (3), then we have

$$\mathbb{Y}_\varepsilon^+ \subset \vec{w}_1 \mathcal{Y}_\varepsilon^+ \oplus \ldots \oplus \vec{w}_{N-1} \mathcal{Y}_\varepsilon^+ .$$

Thus, each component of a function in $\mathbb{Y}_\varepsilon^+$ has patterns as in the binary case and satisfies a wavelength estimate as in Theorem 2.1. This time however, two different phenomena can be observed during the spinodal decomposition process, depending on the homogeneous initial concentration $\bar{u}_o \in \mathcal{G}$.

First, it is possible that the eigenvalue curves corresponding to several β_k's have the same magnitude. In this case, solutions starting near the equilibrium decompose in such a way that the local concentrations of the alloy are driven away from $\bar{u}_o$ in many directions. This is made precise in the following theorem.

Theorem 5.1 *Let $\beta_1 = \beta_2 = \ldots = \beta_{i^*} \gg \beta_{i^*+1} \geq \ldots \geq \beta_{N-1}$ denote the eigenvalues of B for the linearization of the multi-component Cahn-Hilliard system (7) at the unstable homogeneous equilibrium $\bar{u}_o$. Then on a neighborhood of $\bar{u}_o$ with size proportional to $\varepsilon^{\dim \Omega}$ as $\varepsilon \to 0$, the subspace $\mathbb{Y}_\varepsilon^+$ dominates the behavior of all solutions of (7) originating near $\bar{u}_o$. Moreover, the space $\mathbb{Y}_\varepsilon^+$ is contained in $\vec{w}_1 Y_\varepsilon^+ \oplus \ldots \oplus \vec{w}_{i^*} Y_\varepsilon^+$.*

If on the other hand $\beta_1 \gg \beta_2$, one observes a strong mutual coupling of the components. That is, since the dominating subspace is unidirectional, one observes a linear relationship in the mixtures of the components. By virtue of being a separation into two states in opposite directions along a line, this situation is called *pseudo-binary*. Note however that the two states of separation are not pure concentrations of two of the N metals. More precisely, we have the following result concerning the structure of the dominating subspace $\mathbb{Y}_\varepsilon^+$, which is responsible for the occurrence of pseudo-binary decomposition.

Theorem 5.2 *Suppose the eigenvalues of B satisfy $\beta_1 \gg \beta_2 \geq \ldots \geq \beta_{N-1}$. Then on a neighborhood of the unstable homogeneous equilibrium $\bar{u}_o$ with size proportional to $\varepsilon^{\dim \Omega}$ the subspace $\mathbb{Y}_\varepsilon^+ \subset \vec{w}_1 Y_\varepsilon^+$ is dominant. Thus, all components of the elements of $\mathbb{Y}_\varepsilon^+$ are constant multiples of each other. Functions of this form are called pseudo-binary.*

Figure 5 illustrates the two cases described in Theorems 5.1 and 5.2 for ternary alloys, i.e., for $N = 3$, and the potential F defined in (8), as a function of the parameter σ. As mentioned above, the shaded regions of each Gibbs triangle $\mathcal{G}$ are the regions for which the equilibria are unstable, and thus exhibit spinodal decomposition. In (a) and (b), all equilibria cause pseudo-binary decomposition. The lines marked denote the direction of the linear separation for fixed mass being the dots marked. In (c), spinodal decomposition for equilibria in the darker region is not pseudo-binary. Instead, the solutions move away from the equilibrium in all directions, and there is no obvious ordered separation; this is the behavior described in Theorem 5.1.

Together with David Eyre we are currently working to generalize the later stage results to the multi-component system as well. Other extensions of these results are to the Cahn-Hilliard lattice system with discretized spatial lattice, as in Maier-Paape, Moore, Van Vleck [23], and to the stochastic Cahn-Hilliard-Cook model, see Blömker, Maier-Paape, Wanner [3]. Cahn-Hilliard-type convolution equations also show promise.

In addition to furnishing an explanation for the Cahn-Hilliard equation, the methods apply quite well to a number of related equations and models. Specifically, reaction-diffusion systems arising in biological applications with similar spectral properties appear to show similar signs of being driven into an unexpectedly linear regime near equilibrium, despite strong nonlinearities. Sander and Wanner are currently working towards such results.

References

[1] F. Bai, C. M. Elliott, A. Gardiner. A. Spence, and A. M. Stuart. The viscous Cahn-Hilliard equation. Part I: Computations. *Nonlinearity*, 8:131–160, 1995.

[2] F. Bai, A. Spence, and A. M. Stuart. Numerical computations of coarsening in the one-dimensional Cahn-Hilliard model of phase separation. *Physica D*, 78:155–165, 1994.

[3] D. Blömker, S. Maier-Paape, and T. Wanner. Spinodal decomposition for the stochastic Cahn-Hilliard equation. *In preparation*, 1999.

[4] J. F. Blowey and C. M. Elliott. The Cahn-Hilliard gradient theory for phase separation with nonsmooth free energy. I. Mathematical analysis. *European Journal of Applied Mathematics*, 2:233–280, 1991.

[5] J. F. Blowey and C. M. Elliott. The Cahn-Hilliard gradient theory for phase separation with nonsmooth free energy. II. Numerical analysis. *European Journal of Applied Mathematics*, 3:147–179, 1992.

[6] J. W. Cahn. Free energy of a nonuniform system. II. Thermodynamic basis. *Journal of Chemical Physics*, 30:1121–1124, 1959.

[7] J. W. Cahn. Phase separation by spinodal decomposition in isotropic systems. *Journal of Chemical Physics*, 42:93–99, 1965.

[8] J. W. Cahn. Spinodal decomposition. *Transactions of the Metallurgical Society of AIME*, 242:166–180, 1968.

[9] J. W. Cahn and J. E. Hilliard. Free energy of a nonuniform system I. Interfacial free energy. *Journal of Chemical Physics*, 28:258–267, 1958.

[10] M. I. M. Copetti. *Numerical analysis of nonlinear equations arising in phase transition and thermoelasticity.* PhD thesis, University of Sussex, 1991.

[11] M. I. M. Copetti and C. M. Elliott. Kinetics of phase decomposition processes: Numerical solutions to Cahn-Hilliard equation. *Materials Science and Technology*, 6:273–283, 1990.

[12] K. R. Elder and R. C. Desai. Role of nonlinearities in off-critical quenches as described by the Cahn-Hilliard model of phase separation. *Physical Review B*, 40:243–254, 1989.

[13] K. R. Elder, T. M. Rogers, and R. C. Desai. Early stages of spinodal decomposition for the Cahn-Hilliard-Cook model of phase separation. *Physical Review B*, 38:4725–4739, 1988.

[14] C. M. Elliott. The Cahn-Hilliard model for the kinetics of phase separation. In J. F. Rodrigues, editor, *Mathematical Models for Phase Change Problems*, pages 35–73. Birkhäuser, Basel, 1989.

[15] C. M. Elliott and D. A. French. Numerical studies of the Cahn-Hilliard equation for phase separation. *IMA Journal of Applied Mathematics*, 38:97–128, 1987.

[16] D. J. Eyre. Systems of Cahn-Hilliard equations. *SIAM Journal on Applied Mathematics*, 53:1686–1712, 1993.

[17] D. J. Eyre. Cascades of spinodal decompositions in the ternary Cahn-Hilliard equations. In L. Q. Chen, B. Fultz, J. W. Cahn, J. R. Manning, J. E. Morral, and J. A. Simmons, editors, *Mathematics of Microstructure Evolution*, pages 367–378. The Minerals, Metals & Materials Society, 1996.

[18] P. C. Fife. Models for phase separation and their mathematics. *Preprint*, 1991.

[19] C. P. Grant. Spinodal decomposition for the Cahn-Hilliard equation. *Communications in Partial Differential Equations*, 18:453–490, 1993.

[20] J. E. Hilliard. Spinodal decomposition. In H. I. Aaronson, editor, *Phase Transformations*, pages 497–560. American Society for Metals, Metals Park, Ohio, 1970.

[21] J. M. Hyde, M. K. Miller, M. G. Hetherington, A. Cerezo, G. D. W. Smith, and C. M. Elliott. Spinodal decomposition in Fe-Cr alloys: Experimental study at the atomic level and comparison with computer models. *Acta metallurgica et materialia*, 43:3385–3426, 1995.

[22] J. S. Langer. Theory of spinodal decomposition in alloys. *Annals of Physics*, 65:53–86, 1971.

[23] S. Maier-Paape, B. Moore, and E. Van Vleck. Spinodal decomposition in discrete Cahn-Hilliard equations. *In Preparation*, 1999.

[24] S. Maier-Paape, B. Stoth, and T. Wanner. Spinodal decomposition for multi-component Cahn-Hilliard systems. Preprint 603, Universität Bonn, Sonderforschungsbereich 256, 1999. Submitted for publication.

[25] S. Maier-Paape and T. Wanner. Spinodal decomposition for the Cahn-Hilliard equation in higher dimensions. Part I: Probability and wavelength estimate. *Communications in Mathematical Physics*, 195(2):435–464, 1998.

[26] S. Maier-Paape and T. Wanner. Spinodal decomposition for the Cahn-Hilliard equation in higher dimensions: Nonlinear dynamics. *Archive for Rational Mechanics and Analysis*, to appear.

[27] J. E. Morral and J. W. Cahn. Spinodal decomposition in ternary systems. *Acta metallurgica*, 19:1037–1045, 1971.

[28] E. Sander and T. Wanner. Monte Carlo simulations for spinodal decomposition. *Journal of Statistical Physics*, 95(5–6), 1999. To appear.

[29] E. Sander and T. Wanner. Unexpectedly linear behavior for the Cahn-Hilliard equation. Technical Report TR99-01, University of Maryland, Baltimore County, 1999. Submitted for publication.